sciendo
Power Electronics and Drives
Volume 9(44), 2024 DOI: 10.2478/pead-2024-0031

Decoupled Control of an Active Power Filter in a Vibrating Reference Frame

Research paper

Sebastian Wodyk*, Grzegorz Iwański

Warsaw University of Technology, Institute of Control and Industrial Electronics, 00-662 Warszawa, Poland

Received: 07 June 2024; Accepted: 16 September 2024

Abstract: Active power filter (APF) control is a natural area of application for vibrating reference frame (VRF) transformation due to the intentional occurrence of higher harmonics in the active filter current compensating load current harmonics. Due to the vibrating frame transformation, the APF current can be represented by the DC values, and thus proportional-integral (PI) controllers are sufficient to control the converter current. However, in the typical approach, it may be impossible to combine harmonic filtration with reactive power compensation features, due to the transformation constraints. The solution to this issue is decoupling of the fundamental harmonic and high harmonic components and a separate control for each of them. This paper presents a decoupled control system of an APF, which uses VRF transformation for accurate control of high-current harmonics. Decoupling is a groundbreaking improvement of the VRF method. Moreover, different current limitation scenarios are proposed, considering both harmonics compensation and fundamental frequency reactive current compensation. Theoretical considerations are supported by simulation and experimental tests.

Keywords: *active power filter control • current limitation • delay compensation • non-sinusoidal quantities • vibrating coordinates transformation*

1. Introduction

Harmonics are a significant problem for the power grid, which is increasingly being penetrated by switched power supply units, not only in the industry, but also in household appliances, lighting systems, computers and others. Nowadays, power systems face new challenges, i.e. electric vehicles charging as well as distributed generation from photovoltaic (PV) plants, which may operate in an unstable manner and deteriorate power quality and power grid reliability (Li, 2018). Therefore, devices mitigating unfavourable phenomena such as harmonics or reactive power are necessary for the modern power grid.

Active power filters (APFs) are superior to passive filters since they feature better filtering performance and flexibility as well as smaller weight and volume (Akagi, 2005). One of the most popular approaches is shunt filtering, where APF is connected parallel to the load, as shown in Figure 1. Shunt APF, apart from current harmonics filtration, can compensate and inject reactive power into the grid. Although APF is usually located close to the load and works on its current, in general, reference may be set arbitrarily, to compensate other loads in a local system, especially in terms of reactive power.

The performance of APF depends on both the load harmonics extraction algorithm and the current control system (Asiminoael et al., 2007). Load harmonic current detection can be performed in many ways, e.g. high-pass (or low-pass) filtering of a load current in a synchronous *dq* reference frame (Hu et al., 2012; Lascu et al., 2009) as instantaneous power components *pq* (Akagi et al., 1986), or band-pass filtering of a load current in a stationary $\alpha\beta$ reference frame (Płatek and Osypiński, 2016). Each method has its advantages and disadvantages. Band-pass filtering requires dynamic terms for each harmonic that is considered to be filtered, the number of these terms

* Email: sebastian.wodyk.dokt@pw.edu.pl

Open Access. © 2024 Wodyk and Iwański, published by Sciendo. This is an open access article licensed under the Creative Commons Attribution License (http://creativecommons.org/licenses/by/4.0/).

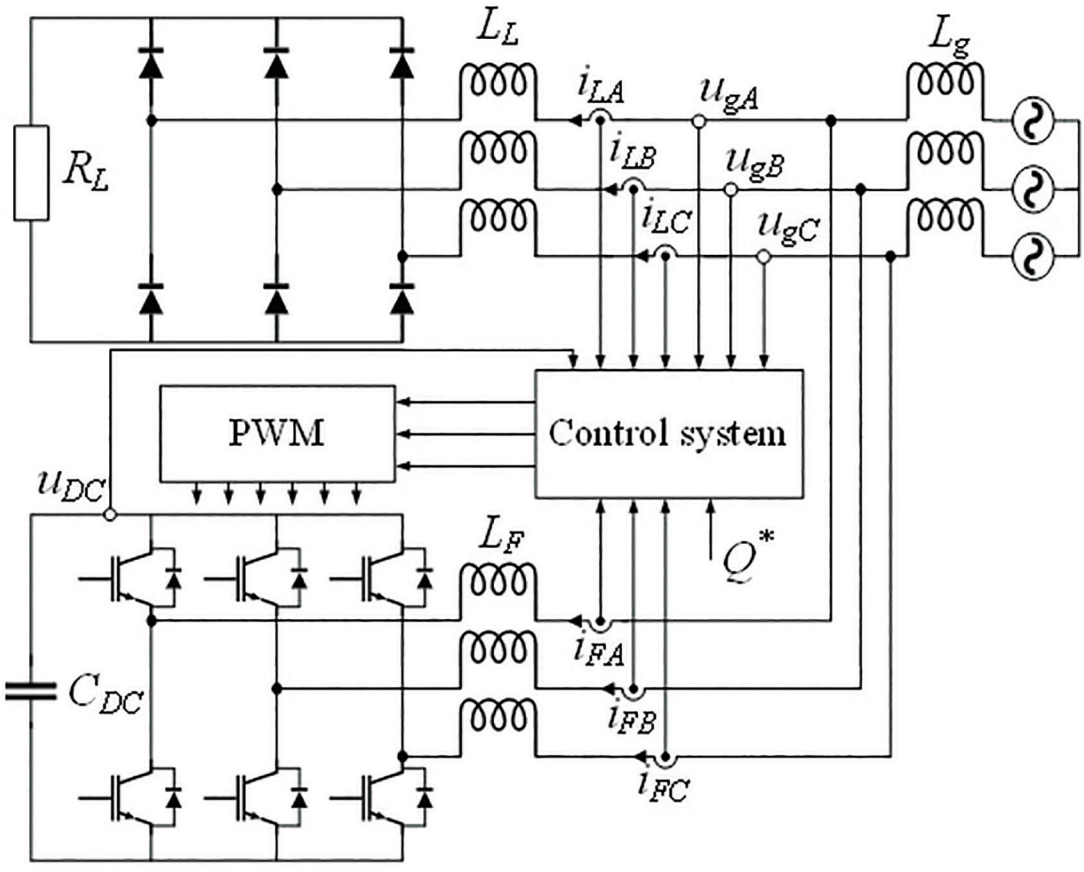

Figure 1. Scheme of a shunt APF operating with a six-pulse diode rectifier. APF, active power filter; PWM, pulse width modulation.

is finite and limited by the computing power of the controller implementing the control algorithm. On the other hand, it gives better accuracy in detecting the harmonics of low order e.g. 5th and 7th, which may be deteriorated using high-pass or low-pass filters in *dq* frame or *pq* power components. In such a system, there is always a trade-off between dynamics and accuracy. A faster response requires a higher cut-off frequency of the filter, which worsens the accuracy of the harmonics extraction due to less attenuation. Additionally, high-frequency noise may be transferred into the reference. However, the advantage of such a system is simplicity, i.e., a low number of dynamic terms.

Accurate tracking of the reference built with harmonics is not trivial. The classical approach with proportional-integral (PI) controllers cannot achieve zero steady-state error for non-DC reference due to the finite gain for AC signals. Theoretically, infinite gain for selected AC signals may be achieved with proportional-resonant (PR) controllers (França et al., 2022), or by the transformation of every harmonic to its synchronous reference frame (multiple reference frame) (Śleszyński et al., 2018). One of the drawbacks of these methods is the necessity for tuning several parallel-connected terms, which is challenging (Ufnalski et al., 2022). Another issue is the realisation of anti-windup, which requires additional structures in each controller term (Amerise et al., 2020). Moreover, for a multiple reference frame approach, there is a need for feedback current decomposition, which deteriorates control dynamics.

It should be noted that converter current may be transformed also to the non-Cartesian reference frame, which is known from the control of a converter during asymmetrical voltage sags (Iwański et al., 2019). The development of non-Cartesian methods brought a vibrating reference frame (VRF) transformation, which allows the transformation of harmonics into a sinusoidal signal, and further into a DC signal in a new *d'q'* frame. Thus, infinite gain can be achieved with PI controllers, ensuring simple anti-windup (Wodyk and Iwanski, 2022).

An APF control may be also realised using non-linear methods, like dead-beat control (Pichan et al., 2022) or sliding-mode control (Ouchen et al., 2021), which ensures fast dynamic response and good reference tracking.

Nevertheless, such methods are vulnerable to system parameters' identification and measurement noise. They also impose a high computational burden.

The digital character of the control system imposes issues related to delays (Hu et al., 2012; Jiang et al., 2018). This problem is unavoidable in digital control systems because of their nature. Moreover, this phenomenon has a particularly strong influence on APFs. As they operate with harmonics, constant delay imposes a different phase shift for each harmonic, which is greater when the order of the harmonic is higher. In order to mitigate this effect, switching frequency, as well as sampling frequency should be as high as possible. Another approach is to use a specific algorithm that compensates for this delay (Pichan et al., 2022).

In Wodyk and Iwanski (2023), the authors proposed the APF control system based on transformation to the VRF, as regulation of quantities composed of different frequencies is a natural implementation area for the mentioned transformation. Nevertheless, this concept is still being developed and researched to overcome drawbacks, keeping the current control loop as simple as possible, which means utilising only PI controllers. For this purpose, a novel decoupled VRF control system is proposed in this paper.

Decoupling ensures independent control of fundamental harmonic and high harmonics. The fundamental part is responsible for DC-link voltage regulation and reactive power and is controlled in the classical synchronous *dq* frame. Harmonics are transformed into the VRF, and then to the synchronous reference frame. It is necessary because in the original approach forcing the fundamental component may lead to unstable operation of APF in some regions. Decoupling is a breakthrough step for the VRF as it allows achieving simultaneous operation with harmonics and fundamental current components, still utilising only PI controllers. Thus, it is a universal tool for three-phase converters.

Another issue discussed in this paper is compensation for the delay caused by the digital implementation of the algorithm, which improves system performance, overcoming the problems mentioned above. Thanks to that, current harmonics can be tracked accurately, which is especially important for high orders. Lack of accuracy may lead even to the amplification of a specific harmonic.

Next, here, limitation of APF current is taken into account, providing different limitation priorities depending on the needs. This issue is consequently neglected by the authors even though it is relevant from the practical point of view not only in terms of converter design but also overcurrent protection or wiring.

This paper discusses a comprehensive approach to an APF control using novel improvements of a VRF, like decoupling and delay compensation, presenting both steady and dynamic states as well as current limitations.

2. APF Reference Current Calculation and Limitation

The APF current consists of three components: fundamental harmonic active components i_{F1d}, fundamental harmonic reactive component i_{F1q} and high harmonic component i_{Fh}. An active component of fundamental current reference i^*_{F1d} is the result of DC-link voltage regulation, as presented in Figure 2. The measured DC-link voltage is filtrated with a 150 Hz low-pass filter to reduce the impact of harmonics on regulation performance. It is known that DC-link voltage regulation is crucial in APF systems, thus its performance may be increased using sophisticated methods, e.g. bi-sliding mode PI control (Li et al., 2022), nevertheless, this paper focuses on AC current regulation and the described simple PI-based method is sufficient.

The output of the PI controller is limited in such a way that i^*_{F1d} cannot exceed the maximum root mean square (RMS) current value I_{rmsMAX} multiplied by √2, which corresponds to the maximum allowable fundamental component amplitude.

Further, the reference reactive component of the fundamental current i^*_{F1q} as well as the reference harmonic current i^*_{Fh} need to be designated. This requires the detection and decomposition of load current, as presented in Figure 3. Current decomposition may be done in various ways, e.g. using multiple second-order generalised

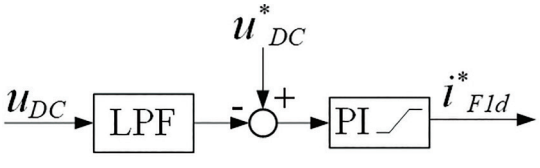

Figure 2. DC-link voltage regulation of the APF. APF, active power filter. PI, proportional-integral.

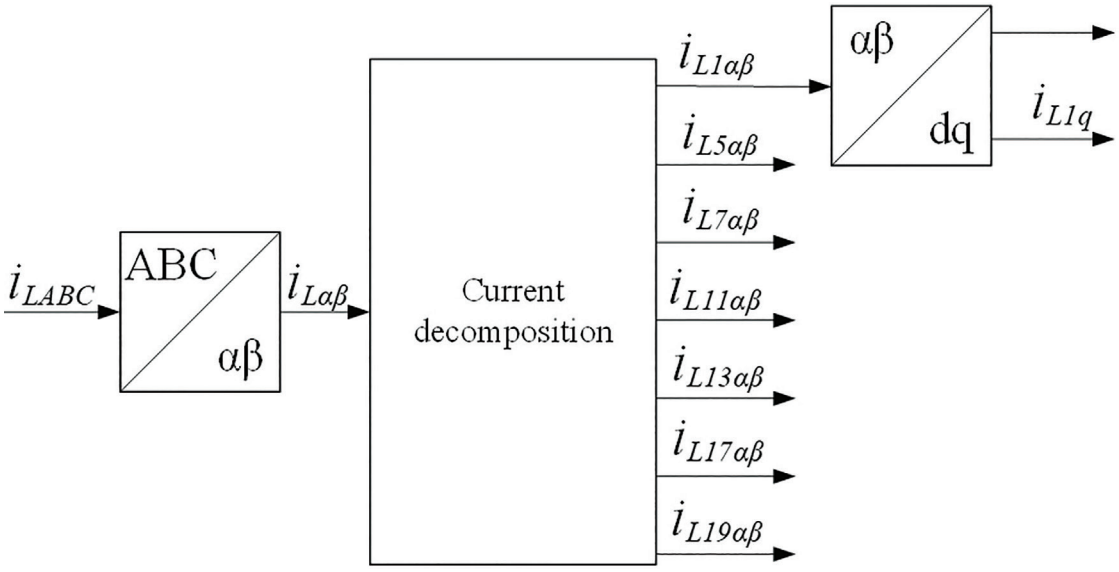

Figure 3. Decomposition of load current.

integrator (MSOGI) (Karbasforooshan and Monfared, 2020) or feedback-based bandpass filters (Wodyk and Iwanski, 2022). Furthermore, an additional reactive component may be set arbitrarily if there is a need for additional reactive power Q^* compensation.

Based on decomposed load current as well as external Q^* reference and DC-link voltage controller output current, limitation is performed. There are three possible scenarios of current limitation, assuming that DC-link voltage maintenance, hence active power always has the highest priority:

1. Load current harmonics compensation priority;
2. Load current reactive component compensation priority;
3. Proportional limitation of a reactive component and harmonic component corresponding to the reference.

A specific scenario should be customised to the needs, although the paper presents the manner of execution of all three limitation methods in Figure 4. The idea is to recalculate the reference of each component based on their RMS values. At first, the maximal possible RMS value of harmonic and reactive components needs to be designated based on the i^*_{F1d}. It is important to ensure an appropriate DC-link voltage level, although in practice it will be a dominating component only during the start-up. An example of the operation of each method is presented in Section V.

Reference APF current is calculated in a stationary $\alpha\beta$ reference frame, as shown in Figure 5. Fundamental harmonic and higher harmonics are designated separately.

3. Direct and Inverse Transformation

As stated in Wodyk and Iwanski (2023), the direct transformation matrix to the vibrating coordinates frame takes the form (1). Apparently, it takes into account the transformation of only the harmonic current component. Thanks to that, fundamental harmonic does not affect the transformation, which reduces the risk of denominator zero crossing.

$$T = \frac{i_{hbase}}{\left|u_{g1}\right|\left(i^*_{Fh\alpha}i^{*q}_{Fh\beta} - i^{*q}_{Fh\alpha}i^*_{Fh\beta}\right)}\begin{bmatrix} u_{g1\alpha}i^{*q}_{Fh\beta} - u_{g1\beta}i^*_{Fh\beta} - u_{g1\alpha}i^{*q}_{Fh\alpha} + u_{g1\beta}i^*_{Fh\alpha} \\ u_{g1\alpha}i^*_{Fh\beta} + u_{g1\beta}i^{*q}_{Fh\beta} - u_{g1\alpha}i^*_{Fh\alpha} - u_{g1\beta}i^{*q}_{Fh\alpha} \end{bmatrix} \tag{1}$$

where: u_{g1}—grid voltage fundamental harmonic, i^*_{Fh}—reference harmonic component of APF current, i^{*q}_{Fh}—reference harmonic component of APF current delayed by $\pi/2$, i_{hbase}—RMS value of i^*_{Fh} scaled by $\sqrt{2}$.

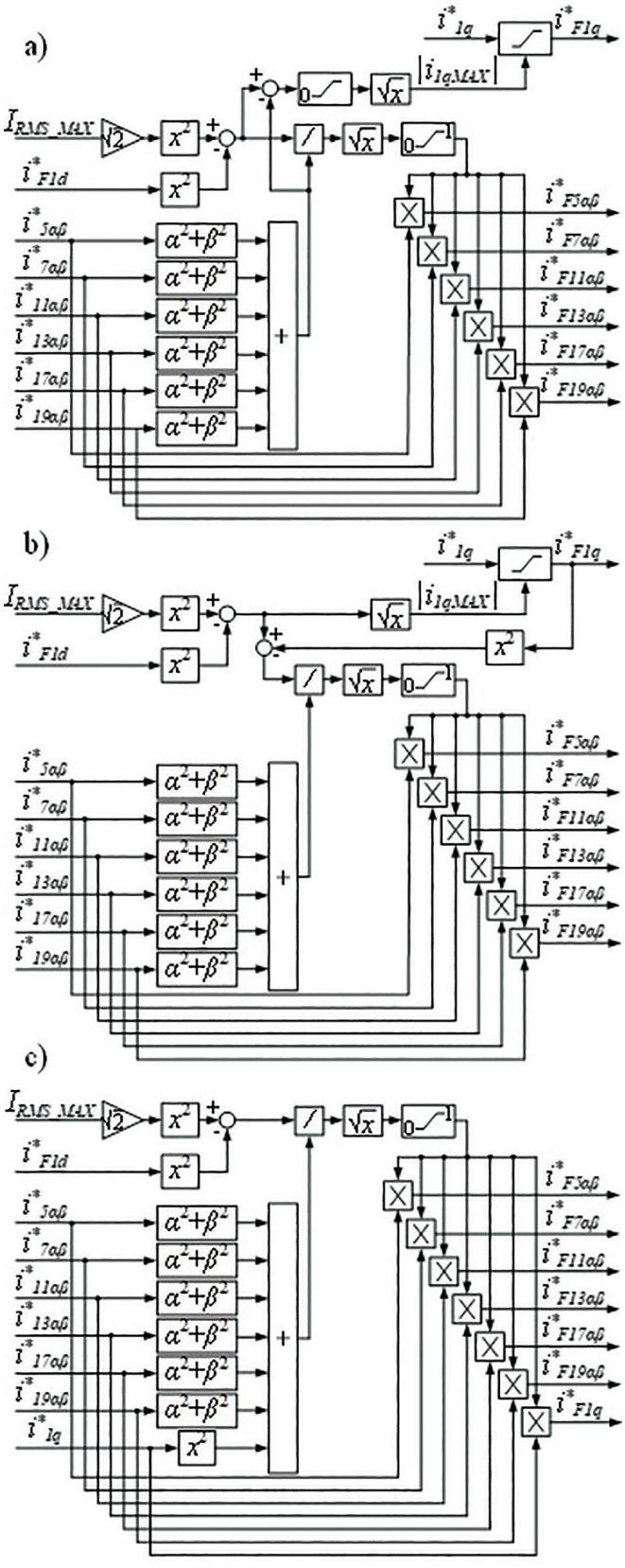

Figure 4. APF current limitation methods: (a) load current harmonics compensation priority, (b) reactive current compensation priority, (c) proportional limitation. APF, active power filter.

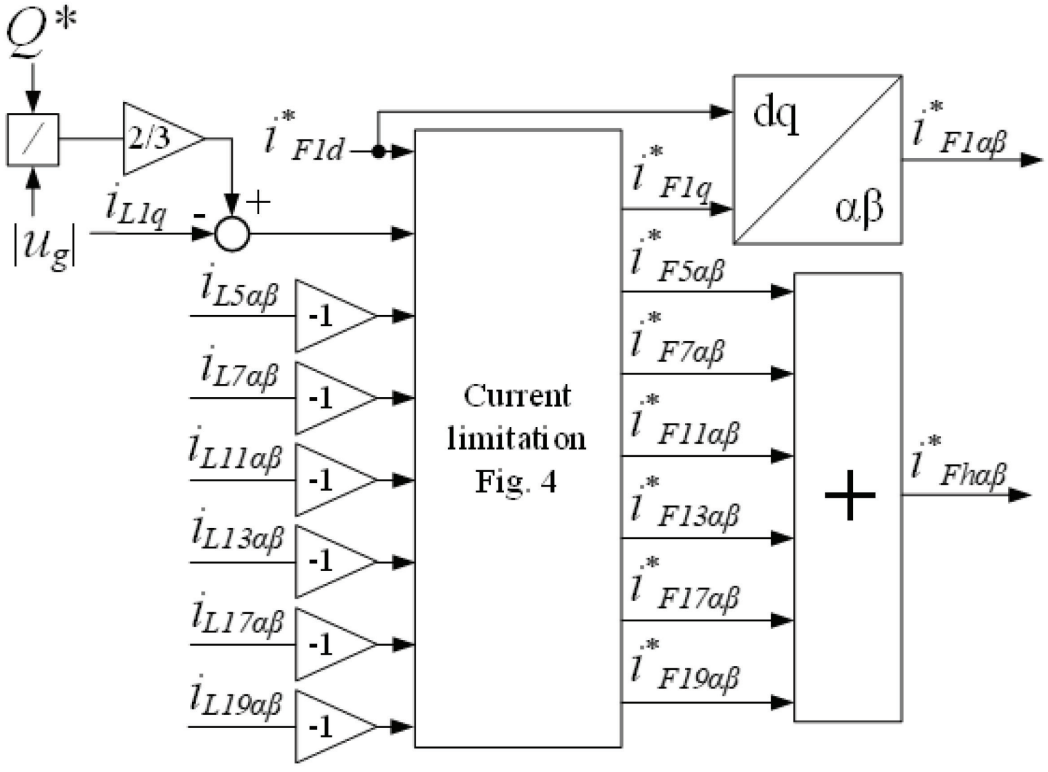

Figure 5. APF reference fundamental current component *i*F1αβ* and harmonic current component *i*Fhαβ* calculation. APF, active power filter.

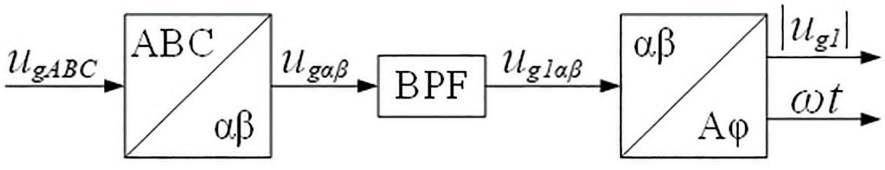

Figure 6. Grid voltage fundamental harmonic extraction and calculation of amplitude and angle.

These parameters can be calculated using Eqs (2)–(4), whereas u_{g1} is provided using the structure presented in Figure 6.

$$i^*_{Fh\alpha} = i^*_{F5\alpha} + i^*_{F7\alpha} + i^*_{F11\alpha} + i^*_{F13\alpha} + i^*_{F17\alpha} + i^*_{F19\alpha} \tag{2a}$$

$$i^*_{Fh\beta} = i^*_{F5\beta} + i^*_{F7\beta} + i^*_{F11\beta} + i^*_{F13\beta} + i^*_{F17\beta} + i^*_{F19\beta} \tag{2b}$$

$$i^{*q}_{Fh\alpha} = -i^*_{F5\beta} - i^*_{F7\beta} + i^*_{F11\beta} + i^*_{F13\beta} - i^*_{F17\beta} - i^*_{F19\beta} \tag{3a}$$

$$i^{*q}_{Fh\beta} = i^*_{F5\alpha} + i^*_{F7\alpha} - i^*_{F11\alpha} - i^*_{F13\alpha} + i^*_{F17\alpha} + i^*_{F19\alpha} \tag{3b}$$

$$i_{hbase} = \sqrt{\left|i^*_{F5}\right|^2 + \left|i^*_{F7}\right|^2 + \left|i^*_{F11}\right|^2 + \left|i^*_{F13}\right|^2 + + \left|i^*_{F17}\right|^2 + \left|i^*_{F19}\right|^2} \tag{4}$$

The result of an inverse transformation is a control signal that corresponds to the voltage drop across filter inductance. Considering that there is a certain delay between sampling of the measured current and updating of the pulse width modulation (PWM) duty cycle, inverse transformation cannot be accurate based on the measured

current directly. This delay has a greater impact on current transformation when the order of the harmonic is greater. It can be described as follows:

$$i_{p\alpha} = |i_p| \cos\left(p\omega(t+T_d)+\theta_p\right) \tag{5a}$$

$$i_{p\beta} = |i_p| \sin\left(p\omega(t+T_d)+\theta_p\right) \tag{5b}$$

$$i_{n\alpha} = |i_n| \cos\left(n\omega(t+T_d)+\theta_n\right) \tag{6a}$$

$$i_{n\beta} = -|i_n| \sin\left(n\omega(t+T_d)+\theta_n\right) \tag{6b}$$

where *p* describes positive sequence harmonics (7th, 13th, 19th, etc.) and *n* describes negative sequence harmonics (5th, 11th, 17th, etc.). As the control system uses current decomposition, an angle of each harmonic of the measured load current may be corrected in the following way:

$$\begin{bmatrix} i^c_{p\alpha} \\ i^c_{p\beta} \end{bmatrix} = \begin{bmatrix} \cos(p\omega T_d) & \sin(p\omega T_d) \\ -\sin(p\omega T_d) & \cos(p\omega T_d) \end{bmatrix} \begin{bmatrix} i_{p\alpha} \\ i_{p\beta} \end{bmatrix} = \begin{bmatrix} |i_p| \cos\left(p\omega t+\theta_p\right) \\ |i_p| \sin\left(p\omega t+\theta_p\right) \end{bmatrix} \tag{7}$$

$$\begin{bmatrix} i^c_{n\alpha} \\ i^c_{n\beta} \end{bmatrix} = \begin{bmatrix} \cos(n\omega T_d) & -\sin(n\omega T_d) \\ \sin(n\omega T_d) & \cos(n\omega T_d) \end{bmatrix} \begin{bmatrix} i_{n\alpha} \\ i_{n\beta} \end{bmatrix} = \begin{bmatrix} |i_n| \cos\left(n\omega t+\theta_n\right) \\ -|i_n| \sin\left(n\omega t+\theta_n\right) \end{bmatrix} \tag{8}$$

It should be noted that trigonometric functions presented in Eqs (7) and (8) may be treated as constant parameters for a given time delay T_d. Using the corrected current harmonics signals, inverse transformation is calculated in the following manner:

$$T_{inv} = \frac{1}{|u_{g1}|\, di_{hbase}} \begin{bmatrix} u_{g1\alpha} di^{*q}_{Fh\alpha} - u_{g1\beta} di^{*}_{Fh\alpha} & u_{g1\alpha} di^{*}_{Fh\alpha} + u_{g1\beta} di^{*q}_{Fh\alpha} \\ u_{g1\alpha} di^{*q}_{Fh\beta} - u_{g1\beta} di^{*}_{Fh\beta} & u_{g1\alpha} di^{*}_{Fh\beta} + u_{g1\beta} i^{*q}_{Fh\beta} \end{bmatrix} \tag{9}$$

where di^{*}_{Fh}, di^{*q}_{Fh}—signals corresponding to the derivative of reference current and its delayed vector, di_{hbase}—RMS value of di^{*}_{Fh}, scaled by $\sqrt{2}$. These parameters can be calculated using Eqs (10)–(12).

$$di^{*}_{Fh\alpha} = 5i^{*C}_{F5\beta} - 7i^{*C}_{F7\beta} + 11i^{*C}_{F11\beta} - 13i^{*C}_{F13\beta} + 17i^{*C}_{F17\beta} - 19i^{*C}_{F19\beta} \tag{10a}$$

$$di^{*}_{Fh\beta} = -5i^{*C}_{F5\alpha} + 7i^{*C}_{F7\alpha} - 11i^{*C}_{F11\alpha} + 13i^{*C}_{F13\alpha} - 17i^{*C}_{F17\alpha} + 19i^{*C}_{F19\alpha} \tag{10b}$$

$$di^{*q}_{Fh\alpha} = 5i^{*C}_{F5\alpha} - 7i^{*C}_{F7\alpha} - 11i^{*C}_{F11\alpha} + 13i^{*C}_{F13\alpha} + 17i^{*C}_{F17\alpha} - 19i^{*C}_{F19\alpha} \tag{11a}$$

$$di^{*q}_{Fh\beta} = 5i^{*C}_{F5\beta} - 7i^{*C}_{F7\beta} - 11i^{*C}_{F11\beta} + 13i^{*C}_{F13\beta} + 17i^{*C}_{F17\beta} + 19i^{*C}_{F19\beta} \tag{11b}$$

$$di_{base} = \sqrt{25\left|i^{*C}_{F5}\right|^2 + 49\left|i^{*C}_{F7}\right|^2 + 121\left|i^{*C}_{F11}\right|^2 + 169\left|i^{*C}_{F13}\right|^2 + 289\left|i^{*C}_{F17}\right|^2 + 361\left|i^{*C}_{F19}\right|^2} \tag{12}$$

A scheme of direct and inverse transformation matrices designation is presented in Figure 7.

4. Current Control System

The proposed decoupled control system of APF is presented in Figure 8. Current regulation is done by using PI controllers, but they are divided into three paths. A proportional controller is applied in a stationary reference

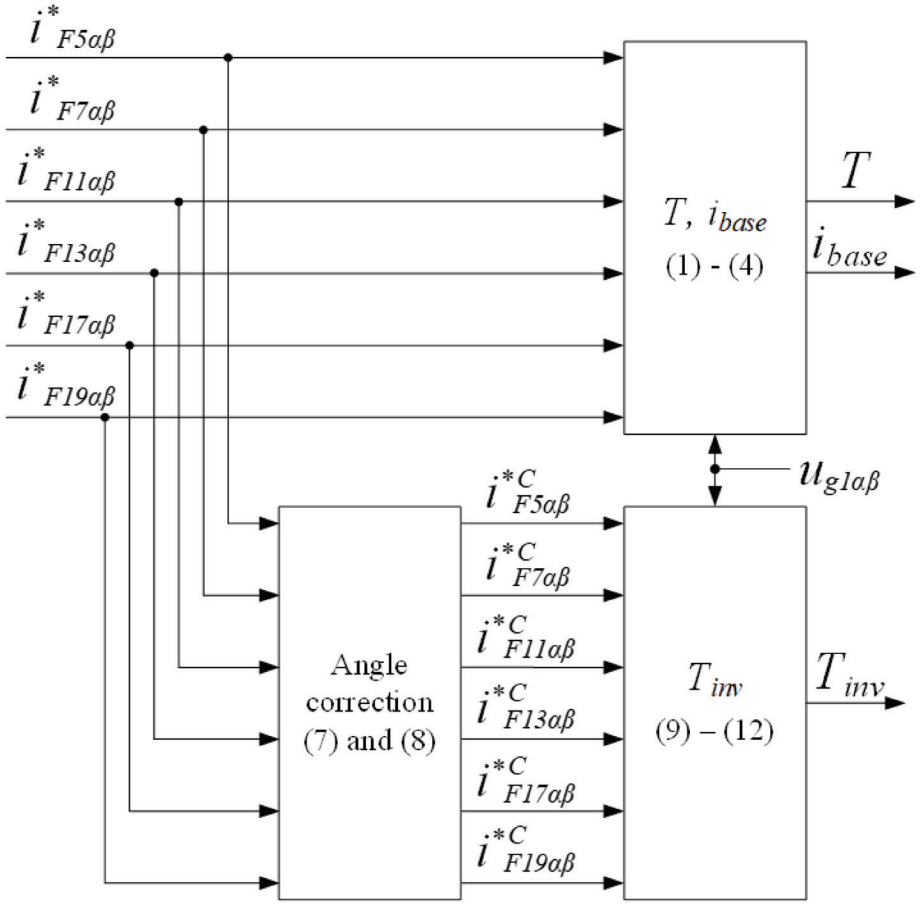

Figure 7. Calculation of direct and inverse transformation matrices.

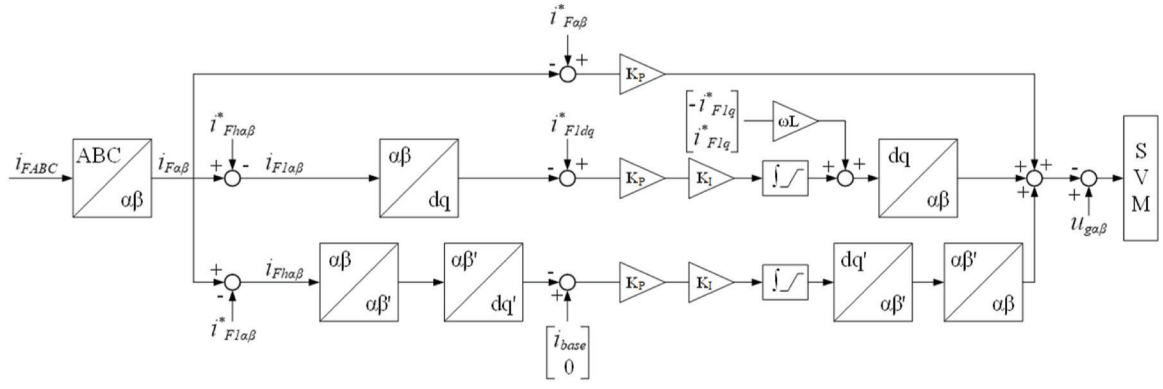

Figure 8. Scheme of the proposed control system.

frame and operates on the whole current. Further, there are two separate integrals for fundamental and harmonic components. The fundamental component is regulated in a classical synchronous *dq* reference frame with decoupling. The harmonic component is regulated in a synchronous reference frame *d'q'* obtained from a VRF *α'β'*.

Decoupling between the fundamental and harmonic components is realised by mutual subtraction of the reference from the measured APF current. A similar approach is known from the double synchronous reference frame control of a grid-connected converter operating with asymmetrical current (Reyes et al., 2012).

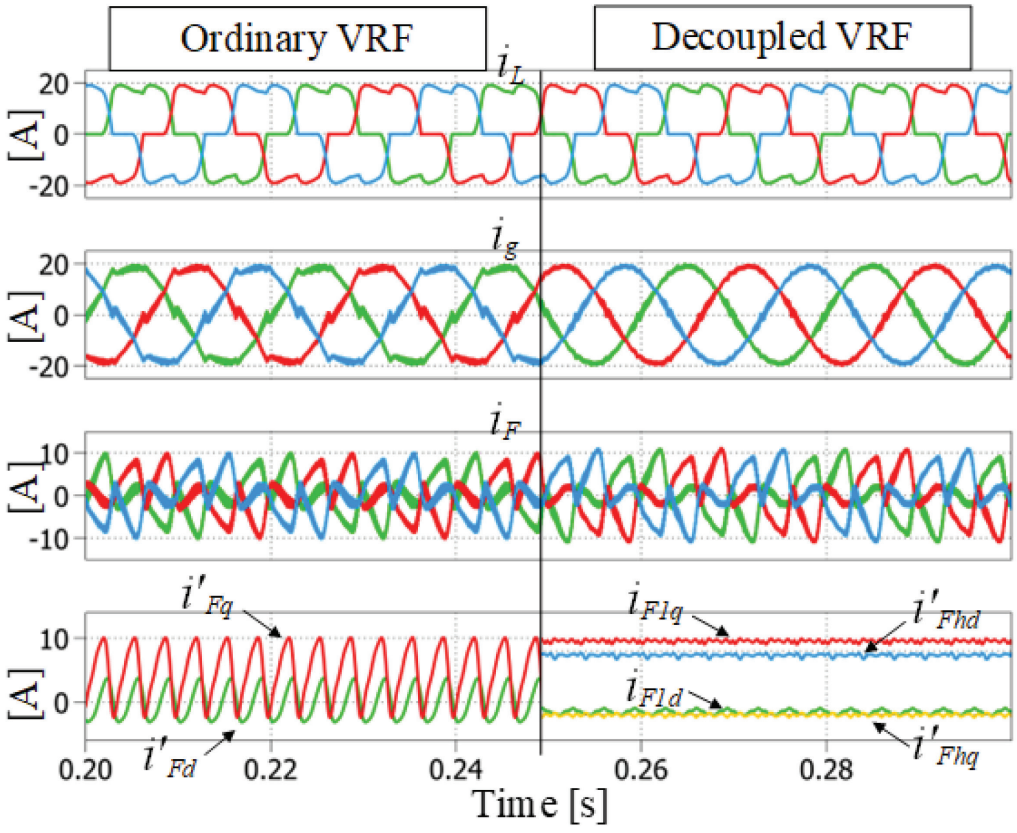

Figure 9. Comparison of ordinary VRF and decoupled VRF for operation with harmonics and reactive power. VRF, vibrating reference frame.

Decoupling allows to mitigate the risk of unstable operation of the VRF, which causes transformation turn-off ($i'_{dq} = i_{dq}$), which is described in Section II-C of Wodyk and Iwanski (2023). This situation may appear when the share of the reference fundamental harmonic grows, e.g. to compensate for the reactive power. Decoupled control can still operate with VRF which is presented in Figure 9.

Outputs of the controllers from each path are summed up. Additionally, grid voltage feedforward is applied, to make controller outputs correspond to the voltage drop on filter inductance without the need to build up the control signal component responsible for grid voltage influence compensation (disturbance rejection loop).

5. Simulation and Experimental Results

Simulation and experimental tests were conducted with the three-phase two-level insulated-gate bipolar transistor (IGBT) converter operating as APF and 6-pulse diode rectifier with resistive load, connected to the grid through an inductive filter. The laboratory rig was configured as presented in Figure 1. The control system was realised with a digital signal processor (DSP) controller built with TMS320F28335. The parameters of the studied circuit are presented in Table 1. In simulation 3 V of 5th harmonic and 3 V of 7th harmonic were added to the grid voltage, which gives 2.5% voltage total harmonic distortion (THD).

Simulation results are presented in Figure 10. Filtering of the harmonics as well as reactive power compensation starts in response to switching on a non-linear load. As can be seen, the current represented in *dq* and *d'q'* frames keeps the DC character in a steady state, which confirms the assumption related to the proposed decoupled VRF control system. Further, the results of the experimental study presented in Figure 11 confirm the practical feasibility of the proposed approach to APF control. It should be noted that the experimental control system implemented in a popular DSP was widely used in the industry. Results presented in Figures 10 and 11 were achieved with delay compensation.

Table 1. Parameters of the simulated circuit and laboratory rig.

Symbol	Quantity	Value
U_{gn}	Nominal grid voltage (L–L RMS)	230 V
$I_{F\_RMS\_MAX}$	Maximal APF RMS current	10 A
L_F	APF chokes inductance	1.7 mH
R_{LF}	APF chokes resistance	40 mΩ
C_{DC}	APF DC-bus capacitance	0.5 mF
U_{DC}	Reference APF DC-bus voltage	410 V
L_L	Load chokes inductance	2 mH
R_L	Load chokes resistance	40 mΩ
L_g	Grid inductance	40 μH
R_g	Grid resistance	1 mΩ
S_L	Rated load power	6.3 kVA
f_s	Switching frequency	10 kHz

APF, active power filter.

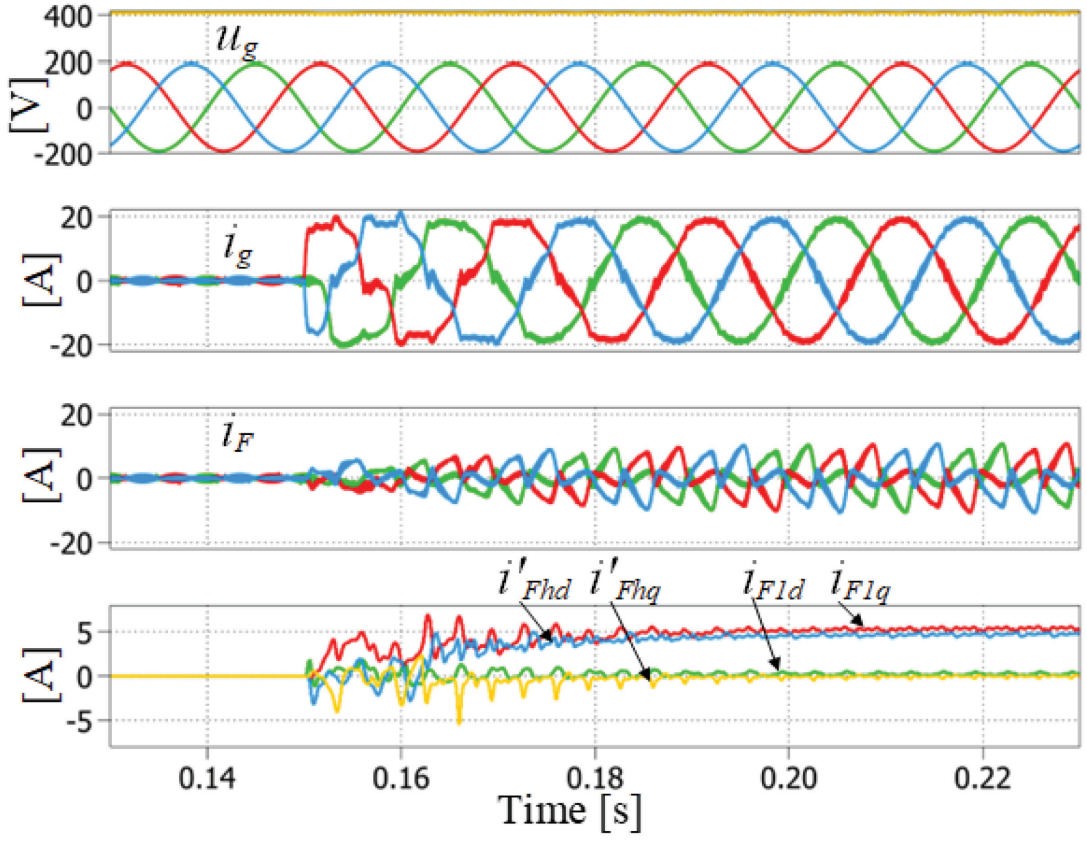

Figure 10. Simulation results presenting performance of APF, u_g—three-phase line-to-neutral grid voltage, i_g—three-phase grid current, i_F—three-phase APF current, i'_{Fhdq}—APF harmonic current in the new $d'q'$ frame, i_{F1dq}—APF fundamental harmonic current in an ordinary dq frame. APF, active power filter.

Figure 12 presents the impact of delay compensation on filtering performance. As can be seen, the current becomes smooth after the turn-on of the compensation grid. Without compensation, VRF integrals cannot be fully accurate, because inverse transformation is calculated for one sample before the actual voltage drop on the inductors. This puts more emphasis on the proportional part which, as shown, cannot eliminate tracking error for higher harmonics. The introduction of the delay compensation effect can also be observed in the fast Fourier

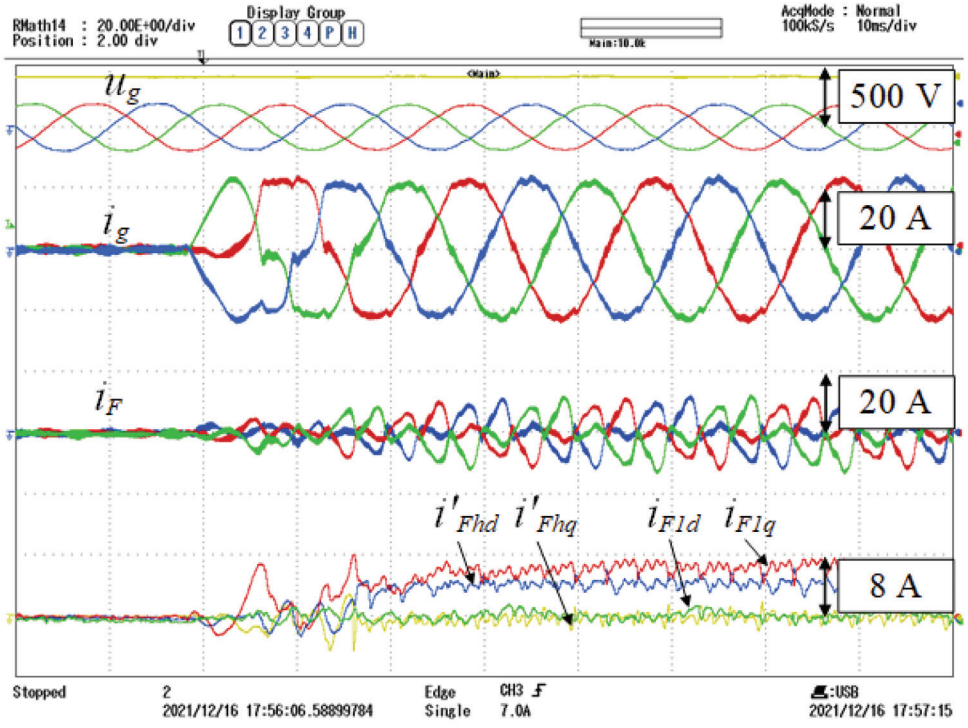

Figure 11. Experimental results presenting performance of APF, u_g—three-phase line-to-neutral grid voltage, i_g—three-phase grid current, i_F—three-phase APF current, i'_{Fhdq}—APF harmonic current in the new *d'q'* frame, i_{F1dq}—APF fundamental harmonic current in an ordinary *dq* frame. APF, active power filter.

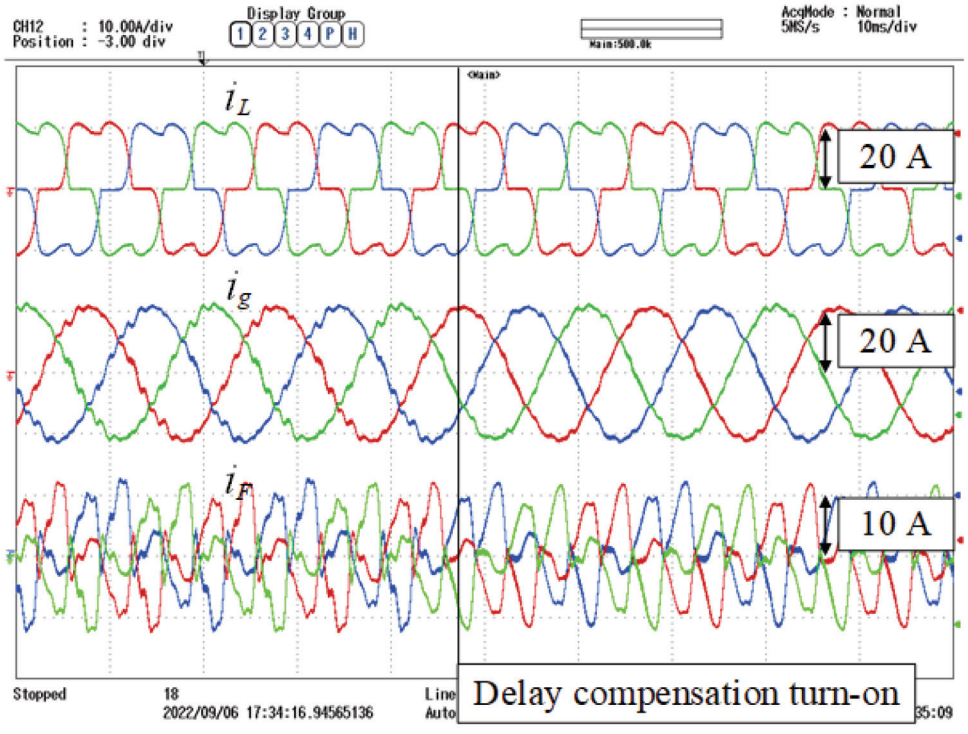

Figure 12. Experimental results presenting impact of the delay compensation on APF performance, i_L—three-phase non-linear load current, i_g—three-phase grid current, i_F—three-phase APF current. APF, active power filter.

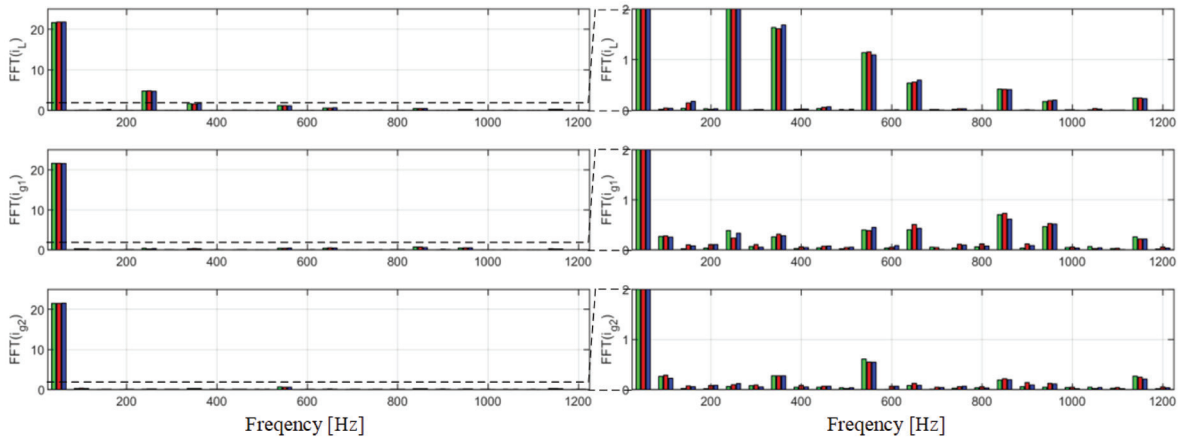

Figure 13. FFT of the measured currents, i_L—load current, i_{g1}—grid current without delay compensation, i_{g2}—grid current with delay compensation.

Table 2. THD of the measured current.

Current	Description	THD (%)
i_{LA}	Load current	24
i_{LB}		24.2
i_{LC}		23.8
i_{g1A}	Grid current without delay compensation	5.5
i_{g1B}		5.9
i_{g1C}		5.5
i_{g2A}	Grid current with delay compensation	3.8
i_{g2B}		3.9
i_{g2C}		3.6

THD, total harmonic distortion.

transform (FFT) analysis presented in Figure 13. As can be seen, the compensation gives considerably better results in the filtration of all harmonics taken into account, apart from 11th. Nevertheless, the current THD is significantly improved, as shown in Table 2.

The proposed current limitation methods performance is presented in Figures 14–16. APF operates with its maximal RMS value, i.e. 10 A. Reference APF current is 3.5 A of the harmonic component RMS value and 14.3 A of the fundamental component RMS value, where 4.3 A resulted from non-linear load reactive power and 10 A was an additional reactive component. The fundamental component reference was capacitive, as opposed to the non-linear load, which has an inductive character due to L_L filter.

The first experiment was conducted for the harmonic current compensation priority method. The results are presented in Figure 14. As the total reference RMS value is greater than the APF limitation, the control system reduces the reactive component, which equals 9.4A, but does not fully compensate for it. Oppositely, APF compensates fully load current higher harmonics according to the selected priority.

Figure 15 presents a case in which reactive current is the highest priority. Then, APF operates with the reactive component only, which equals 10 A of the RMS value, and the grid current contains the whole harmonic component. The current limitation in this test has been intentionally set on a level equal to the reactive current. This is to show that reactive current compensation has full priority. Obviously, a higher current limit will ensure that APF will partially compensate for harmonics.

The next selection of APF current limitation is a proportional limitation of fundamental and harmonic components, corresponding to the reference. Such a case is presented in Figure 16. Both harmonic and reactive components are filtered and compensated partially. For the presented experiment, the harmonic component RMS value equals 2.3 A, whereas the fundamental component RMS value equals 9.7 A.

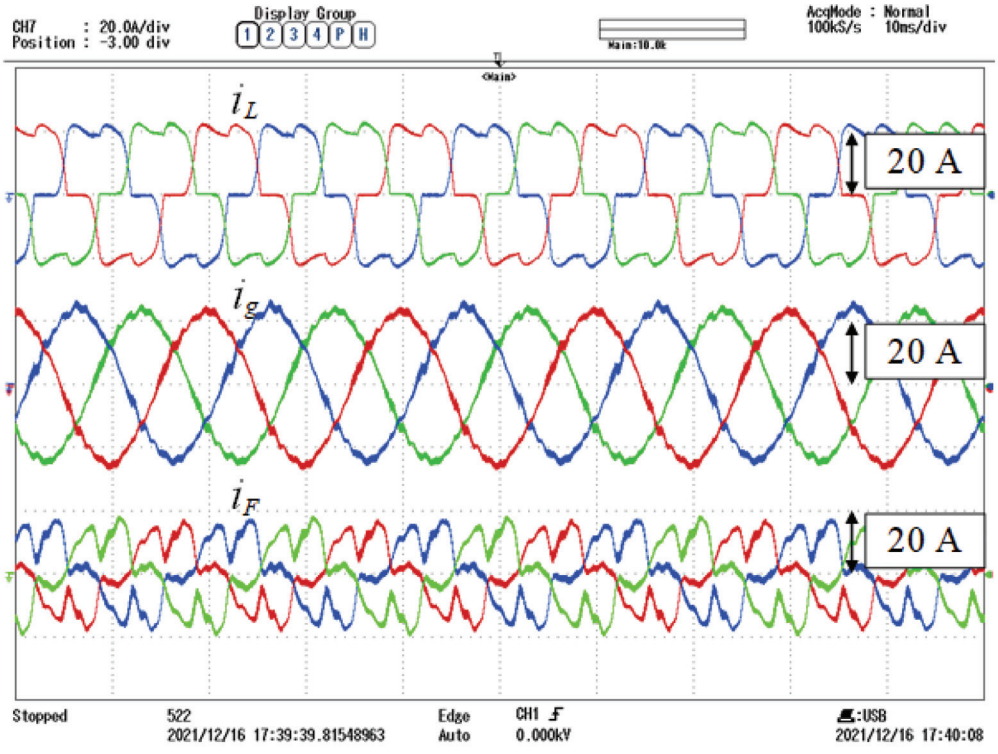

Figure 14. Experimental results presenting current limitation with harmonic current priority, i_L—three-phase non-linear load current, i_g—three-phase grid current, i_F—three-phase APF current. APF, active power filter.

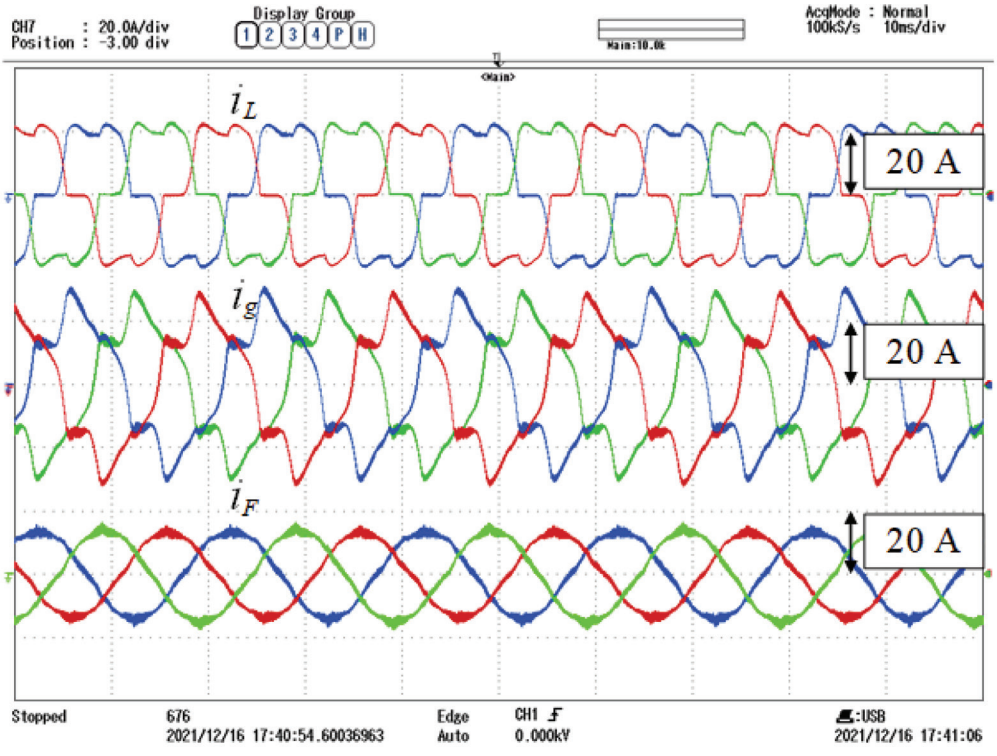

Figure 15. Experimental results presenting current limitation with reactive power current priority, i_L—three-phase non-linear load current, i_g—three-phase grid current, i_F—three-phase APF current. APF, active power filter.

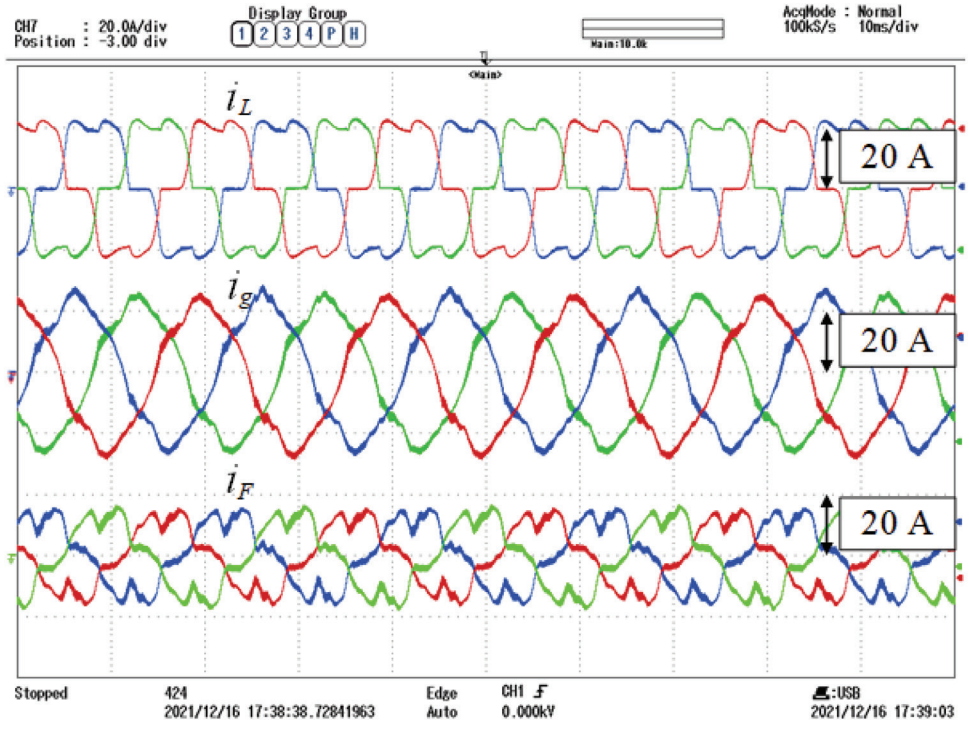

Figure 16. Experimental results presenting proportional current limitation, i_L—three-phase non-linear load current, i_g—three-phase grid current, i_F—three-phase APF current. APF, active power filter.

Each of the presented methods allows us to obtain appropriate limitation of the APF current RMS value. The selection of the specific one depends on various conditions and requires further research. Limitation methods may be developed e.g. by introducing weights for each component or even for each harmonic separately.

Simulation results for the case of a load without inductive filter are presented in Figures 17 and 18. To simulate the worst case, grid impedance was eliminated. As can be seen, a characteristic spike appears in the grid current. It cannot be fully compensated because of limited di/dt of the APF, which depends on DC-link voltage and filter inductance. On the other hand, in general, such a high di/dt is difficult to measure and sample, because it demands a much higher sampling frequency. Compensation is also not trivial due to delays in the control system that may even amplify those spikes.

It should be noted that this is a theoretical situation because in practice the grid inductance is greater than zero. Moreover, such a connection of non-linear loads, without any filter is strongly inadvisable. Diode rectifiers are often connected through a separation transformer, which can be interpreted as an inductive filter due to the leakage inductance. On the other hand, in industrial applications placing an inductive filter is a common approach, and even if the main inductor is placed on the DC side, additional small inductors are added on the AC side to reduce di/dt.

6. Conclusion

The paper presents a novel control system of an APF, using the VRF transformation and decoupling of the fundamental and harmonic current components. Thanks to that both components may be controlled separately, but still using PI controllers. Some improvements of the VRF control were presented like the already mentioned decoupling as well as compensation of the delay introduced by the sampling and PWM, which improves filtering performance due to more accurate current reference tracking.

Another important issue discussed in the paper was the limitation of the APF current RMS value. Three different methods that realise different priorities were presented. Nevertheless, further research in this field can be conducted to specify guidelines for the selection of a specific method that would be optimal for the given application.

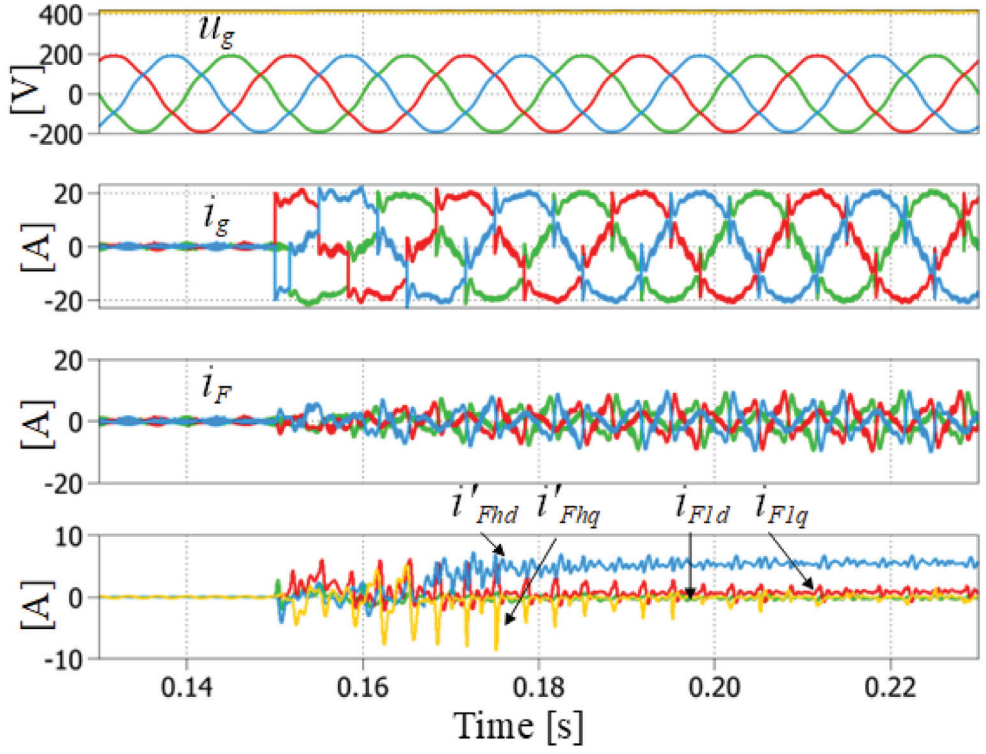

Figure 17. Simulation results presenting performance of APF operating with load with no input filter, u_g—three-phase line-to-neutral grid voltage, i_g—three-phase grid current, i_F—three-phase APF current, i'_{Fhdq}—APF harmonic current in the new *d'q'* frame, i_{F1dq}—APF fundamental harmonic current in an ordinary *dq* frame. APF, active power filter.

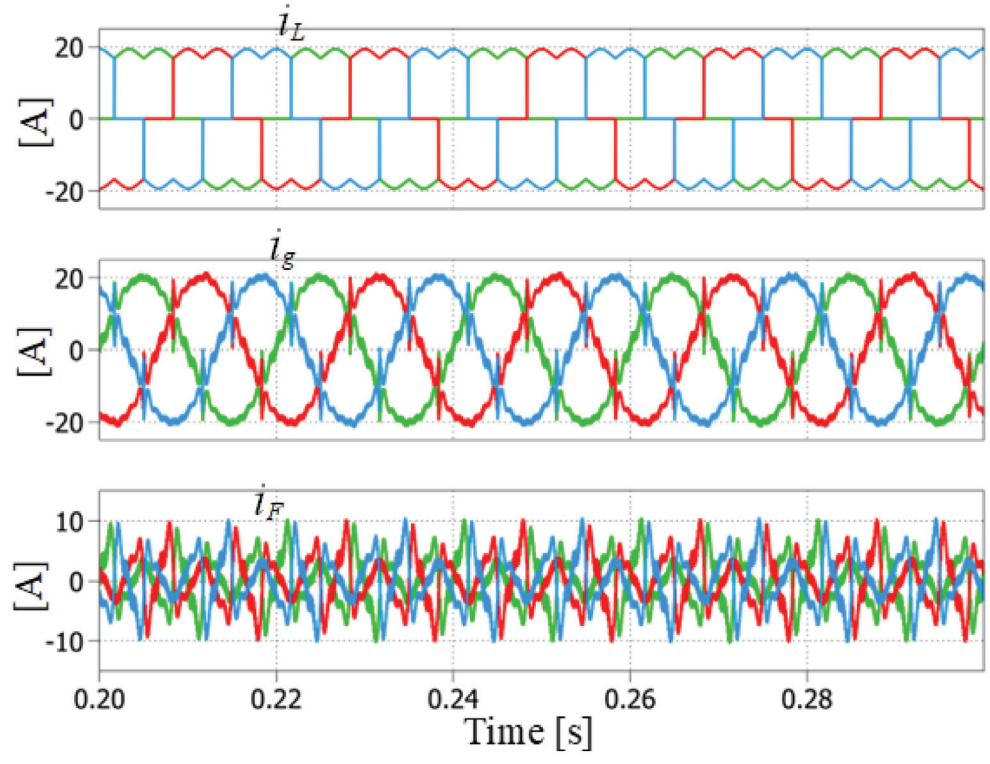

Figure 18. Simulation results presenting currents in the analysed circuit for load with no input filter, i_L—three-phase load current, i_g—three-phase grid current, i_F—three-phase APF current. APF, active power filter.

The proposed control system was examined through both simulation and experimental tests. The experiment was conducted using a DSP TMS320F28335, which is popular in industries, and it proves the practical usefulness and suitability of the proposed method.

Acknowledgements

The Work is supported by the National Science Centre (Poland) within the Project granted on the basis of decision number 2016/23/B/ST7/03942.

Supported by the Foundation for Polish Science (FNP).

References

Akagi, H. (2005). Active Harmonic Filters. *Proceedings of the IEEE*, 93(12), pp. 2128–2141. doi: 10.1109/JPROC.2005.859603

Akagi, H., Nabae, A. and Atoh, S. (1986). Control Strategy of Active Power Filters Using Multiple Voltage-Source PWM Converters. *IEEE Transactions on Industry Applications*, IA-22(3), pp. 460–465. doi: 10.1109/TIA.1986.4504743

Amerise, A., Mengoni, M., Rizzoli, G., Zarri, L., Tani, A. and Casadei, D. (2020). Comparison of Three Voltage Saturation Algorithms in Shunt Active Power Filters with Selective Harmonic Control. *IEEE Transactions on Industry Applications*, 56(3), pp. 2762–2772. doi: 10.1109/TIA.2020.2972853

Asiminoael, L., Blaabjerg, F. and Hansen, S. (2007). Detection is key – Harmonic detection methods for active power filter applications. *IEEE Industry Applications Magazine*, 13(4), pp. 22–33. doi: 10.1109/MIA.2007.4283506

França, B. W., Aredes, M., d. Silva, L. F., Gontijo, G. F., Tricarico, T. C. and Posada, J. (2022). An Enhanced Shunt Active Filter Based on Synchronverter Concept. *IEEE Journal of Emerging and Selected Topics in Power Electronics*, 10(1), pp. 494–505. doi: 10.1109/JESTPE.2021.3103836

Hu, H., Shi, W., Lu, Y. and Xing, Y. (2012). Design Considerations for DSP-Controlled 400 Hz Shunt Active Power Filter in an Aircraft Power System. *IEEE Transactions on Industrial Electronics*, 59(9), pp. 3624–3634. doi: 10.1109/TIE.2011.2165452

Iwański, G., Maciejewski, P. and Łuszczyk, T. (2019). Non-Cartesian Frame Transformation-Based Control of a Three-Phase Power Converter During Unbalanced Voltage Dip – Part I: Transformation Principles. *Power Electronics and Drives*, 4(1), pp. 47–61. doi: 10.2478/pead-2019-0013

Jiang, W., Ding, X., Ni, Y., Wang, J., Wang, L., and Ma W. (2018). An Improved Deadbeat Control for a Three-Phase Three-Line Active Power Filter with Current-Tracking Error Compensation. *IEEE Transactions on Power Electronics*, 33(3), pp. 2061–2072. doi: 10.1109/TPEL.2017.2693325

Karbasforooshan, M. S. and Monfared, M. (2020). An Improved Reference Current Generation and Digital Deadbeat Controller for Single-Phase Shunt Active Power Filters. *IEEE Transactions on Power Delivery*, 35(6), pp. 2663–2671. doi: 10.1109/TPWRD.2020.2974155

Lascu, C., Asiminoaei, L., Boldea, I. and Blaabjerg, F. (2009). Frequency Response Analysis of Current Controllers for Selective Harmonic Compensation in Active Power Filters. *IEEE Transactions on Industrial Electronics*, 56(2), pp. 337–347. doi: 10.1109/TIE.2008.2006953

Li, C. (2018). Unstable Operation of Photovoltaic Inverter from Field Experiences. *IEEE Transactions on Power Delivery*, 33(2), pp. 1013–1015. doi: 10.1109/TPWRD.2017.2656020

Li, Z., Ren, M., Chen, Z., Liu G. and Feng, D. (2022). A Bi-Sliding Mode PI Control of DC-Link Voltage of Three-Phase Three-Wire Shunt Active Power Filter. *IEEE Journal of Emerging and Selected Topics in Power Electronics*, 10(6), pp. 7581–7588. doi: 10.1109/JESTPE.2022.3168313

Ouchen, S., Benbouzid, M., Blaabjerg, F., Betka A. and Steinhart, H. (2021). Direct Power Control of Shunt Active Power Filter Using Space Vector Modulation Based on Supertwisting Sliding Mode Control. *IEEE Journal of Emerging and Selected Topics in Power Electronics*, 9(3), pp. 3243–3253. doi: 10.1109/JESTPE.2020.3007900

Pichan, M., Seyyedhosseini, M. and Hafezi, H. (2022). A New DeadBeat-Based Direct Power

Control of Shunt Active Power Filter with Digital Implementation Delay Compensation. *IEEE Access*, 10(July), pp. 72866–72878. doi: 10.1109/ACCESS.2022.3188685

Płatek, T. and Osypiński, T. (2016). Current Control with Asymmetrical Regular Sampled Pulse Width Modulator Applied in Parallel Active Filter. *Bulletin of the Polish Academy of Sciences: Technical Sciences*, 64(2), pp. 287–300. doi: 10.1515/BPASTS-2016-0033

Reyes, M., Rodriguez, P., Vazquez, S., Luna, A., Teodorescu, R. and Carrasco, J. M. (2012). Enhanced Decoupled Double Synchronous Reference Frame Current Controller for Unbalanced Grid-Voltage Conditions. *IEEE Transactions on Power Electronics*, 27(9), pp. 3934–3943. doi: 10.1109/TPEL.2012.2190147

Śleszyński, W., Cichowski, A. and Mysiak, P. (2018). Current Harmonic Controller in Multiple Reference Frames for Series Active Power Filter Integrated with 18-Pulse Diode Rectifier. *Bulletin of the Polish Academy of Sciences: Technical Sciences*, 66(5), pp. 699–704. doi: 10.24425/125336

Ufnalski, B., Michalczuk, M. and Galecki, A. (2022). Robust Tuning of Multiresonant Current Controllers for Grid-Tied Converters and Erroneous Use of the Naslin Polynomial Method. *IEEE Access*, 10(July), pp. 88211–88225. doi: 10.1109/ACCESS.2022.3199702

Wodyk, S. and Iwanski, G. (2022). Vibrating Coordinates Frame Transformation Based Unity Power Factor Control of a Three-Phase Converter at Grid Voltage Imbalance and Harmonics. *IEEE Transactions on Industrial Electronics*, 69(2), pp. 1114–1123. doi: 10.1109/TIE.2021.3059551

Wodyk, S. and Iwanski, G. (2023). Active Power Filter Control with Vibrating Coordinates Transformation. *IEEE Transactions on Power Delivery*, 38(1), pp. 376–386. doi: 10.1109/TPWRD.2022.3189782